Frontogenesis in a Continuously Varying Potential Vorticity Fluid

G. W. KENT MOORE

Department of Physics, University of Toronto, Toronto, Ontario M5S 1A7

(Manuscript received 23 June 1986, in final form 29 September 1986)

ABSTRACT

The geostrophic momentum approximation and a Lagrangian formulation are employed to consider the nature of the fronts that result from the action of a stretching deformation field in a continuously varying potential vorticity fluid. In such a fluid, the tropopause is represented by a shallow region over which the potential vorticity changes from a representative tropospheric value to a representative stratospheric one. Decreasing the depth of this zone resulted in an increase in the intensity of the upper-level front. Reduction in the cross-front temperature contrast reduced the intensity of both the surface and upper-level front. Most notably it resulted in the elimination of the deep tropopause fold in the vicinity of the upper-level front.

The environment in which the fronts form may have temperature perturbations that are the result of previous or contemporaneous frontogenetic processes. The effects of two different types of perturbations were studied with the continuous model. The inclusion of a barotropic perturbation, i.e. one that is localized in the cross-front direction but that extends throughout the depth of the fluid, resulted in an increase in the intensity of both the surface and upper-level fronts. The upper-level advection of cold air that results in a localized region of reduced potential temperature has been identified as an additional frontogenetic process. In contrast to the effect of the barotropic perturbation, such a localized perturbation resulted in an increase in the intensity of the upper-level front only.

1. Introduction

The problem of two-dimensional frontogenesis, i.e. the development of localized regions of strong horizontal temperature gradients, has been successfully modeled by the application of the geostrophic momentum approximation. Beginning with the work of Hoskins and Bretherton (1972; hereafter HB) it has been demonstrated that with this approximation, realistic frontal zones can develop as the result of the action of geostrophic stretching or shearing deformation fields. These frontal zones have several features in common with synoptic scale fronts. In particular, they are narrow (~800 km wide) sloping baroclinic zones that are most intense at the surface and at the tropopause. In this paper, we will refer to the entire baroclinic zone as the frontal zone, while calling the regions of maximum baroclinicity either the surface or the upper-level front. The earliest models (HB; Hoskins, 1971, hereafter H) considered frontogenesis in a constant potential vorticity fluid and in a "two-layer" fluid. The frontal zones that formed in the constant potential vorticity fluid were symmetric in the sense that the surface and upper-level fronts were of equal strength. The model did not take into account the effects that a deformable tropopause would have on the upper-level front. These effects were included in the latter model which consisted of two layers with very different potential vorticities that represented the troposphere and the stratosphere. In this model, the surface and upper-level fronts were of dramatically different intensities.

The success of the geostrophic momentum approximation in describing the evolution of the synoptic-scale frontal zones is the result of the retention of the ageostrophic advection terms in the expression for the material derivative. Its inclusion allows the horizontal convergence field associated with the ageostrophic circulation to further concentrate the cross-front temperature gradient. The absence of this positive feedback mechanism accounted for the unphysical characteristics of the frontal zones that were generated with the quasi-geostrophic approximation (Stone, 1966; Williams, 1968). Differential vertical motions are, in general, frontolytic and hence the advection process is most effective near rigid boundaries where these motions vanish. In the constant potential vorticity fluid, the vertical velocity is zero at the tropopause as well as at the surface and this leads to the aforementioned symmetry between the surface and upper-level fronts. The inclusion of a deformable tropopause removes the condition that the vertical velocity vanishes there. This frontolytic effect reduces the intensity of the upper-level front and breaks the symmetry between it and the surface front.

Observations by Reed (1955) suggest that tilting effects from a thermally indirect secondary circulation are important in generating upper-level fronts. Strong subsidence on its warm side results in a deep intrusion of stratospheric air into the troposphere. Shapiro (1981) proposed that a shearing deformation field acting on the along-front potential temperature gradient was responsible for the observed indirect circulation. Keyser

and Pecnick (1985) have included this mechanism, albeit in a simplified form, in a two-dimensional model forced by a stretching deformation field. They showed that in cases in which there was cold air advection, a thermally indirect circulation was set up that resulted in an intensification of the upper-level front.

The upper-level fronts generated by a pure stretching deformation field by H had a thermally direct secondary circulation, and as previously mentioned, the vertical motions were frontolytic rather than frontogenetic. To compensate for this, H was forced to employ unrealistic surface temperature distributions in order to obtain realistic upper-level fronts. In particular, he used distributions with cross-frontal surface temperature contrasts of 39°C and 48°C. Observational evidence (Palmen and Newton, 1969) suggests that temperature contrasts across synoptic-scale fronts are on the order of 20°C. It should be noted that Keyser and Pecnick also employed an unrealistic surface cross-front temperature contrast of 40°C. Figure 7 of H shows that initial states with surface temperature distributions that were either monotonic increasing or that had an absolute minimum near the center of the front were employed. The most intense fronts were found to develop on the latter class of initial states. One can show that in the two-layer model the initial tropopause height is determined by the initial surface temperature distribution and that the presence of a temperature minimum implies the existence of a tropopause height minimum. Thus, the initial state in H, upon which the most intense upper-level fronts developed, contained a nascent tropopause fold.

In this paper, we will consider the character of the upper-level fronts that develop on an initial state with a more realistic surface temperature contrast. As was the case with Buzzi et al. (1981), we will consider the process of frontogenesis in a continuously varying potential vorticity fluid. This allows for more flexibility in the choice of an initial potential vorticity distribution than is possible in the two-layer model.

One of the difficulties in attempting to solve this problem is that the potential vorticity is conserved following parcel trajectories, and its value at any given time at any point fixed in space is not necessarily known. The two-layer model of H had a constant potential vorticity in each of the layers, and this difficulty did not arise. Buzzi et al. employed an isentropic coordinate system and because their vertical coordinate was a conserved quantity, the conservation of potential vorticity in their model was particularly simple. However, their choice of vertical coordinate resulted in an elliptic equation for the geopotential that was difficult to solve. A different approach was considered for this investigation. We will employ the same vertical coordinate, the "pseudoheight", that was used by H. This ensures that the elliptic equation for the geopotential has a particularly simple form. We will adopt a Lagrangian formulation to determine the spatial distribution of potential vorticity. By keeping track of the parcel trajectories, we will know where a parcel at any given point originated and hence what its potential vorticity is.

As discussed by Hoskins et al. (1984), the environment in which the fronts form may have perturbations that are the result of previous or contemporaneous frontogenetic processes. Hoskins et al. employed a constant potential vorticity model and hence could only consider perturbations that were localized in the cross-front direction but that extended throughout the depth of the fluid. This type of perturbation will be referred to as a barotropic perturbation. The enhanced upper-level frontogenesis caused by the inclusion by H of a minimum in the surface temperature distribution is an example of such a barotropic perturbation. The use of a continuously varying potential vorticity model allows one to include perturbations that are localized in both spatial directions. As mentioned above, Keyser and Pecnick (1985) investigated frontogenesis in a fluid with an along-front variation in the potential temperature field. They showed that in the case in which there was cold-air advection by the upper-level jet, the development of the upper-level front was intensified. One of the results of this advection should be a region of reduced potential temperature that is localized in the vicinity of the jet core. As will be shown in this paper, this effect can be included in the continuous model by the inclusion of a localized potential vorticity perturbation.

2. Description of the model

The frontal zones that we will consider are assumed to be the result of the action of a geostrophic stretching deformation field. For the purposes of this paper, we will employ a right-handed coordinate system with the x axis in the cross-front direction pointing towards the warmer air and the y axis in the along-front direction. The vertical coordinate is the "pseudoheight" employed by H and defined by

$$z(p) = z_a\left[1 - \frac{p}{p_0}\right]^{(\gamma-1)/\gamma}, \tag{1}$$

where p_0 is the fixed surface pressure (1000 mb), γ is R/C_p (0.286), and z_a is the height of the top of the model atmosphere (28 km). Under the assumption that the along-front length and velocity scales are large compared with the corresponding cross-front scales, the geostrophic momentum approximation (Eliassen, 1948; Hoskins, 1975) may be used to simplify the equations of motion. For the special case in which there is no along-front variation in the temperature field, this approximation reduces the primitive equations to

$$\frac{D}{Dt}\bar{V} + f\bar{U} + \frac{\partial\bar{\phi}}{\partial y} = 0 \tag{2}$$

$$\frac{D\bar{\Theta}}{Dt}=0 \tag{3}$$

$$\frac{g}{\Theta_0}\bar{\Theta}=\frac{\partial\bar{\phi}}{\partial z} \tag{4}$$

$$f\bar{V}=\frac{\partial\bar{\phi}}{\partial x} \tag{5}$$

$$\frac{\partial}{\partial x}\bar{U}+\frac{\partial}{\partial y}\bar{V}+\frac{1}{r}\frac{\partial}{\partial z}r\bar{W}=0, \tag{6}$$

where $(\bar{U}, \bar{V}, \bar{W})$ are the cross-front, along-front, and vertical components of the velocity field; $\bar{\Theta}$ is the potential temperature; $\bar{\phi}$ is the geopotential and r is the pseudodensity

$$r(z)=\rho_0(1-z/z_a)^{1/\gamma}.$$

The material derivative retains the advection by the ageostrophic circulation and is defined by

$$\frac{D}{Dt}=\frac{\partial}{\partial t}+\bar{U}\frac{\partial}{\partial x}+\bar{V}\frac{\partial}{\partial y}+\bar{W}\frac{\partial}{\partial z}.$$

The geostrophic stretching deformation field is assumed to be adequately represented by

$$U_d=-\alpha(t)x$$

$$V_d=\alpha(t)y. \tag{7}$$

The strength of the deformation field α is an arbitrary, albeit slowly varying function of time. For this paper, we will assume that it is the constant $\alpha_0 = 10^{-5}\ \mathrm{s}^{-1}$. As discussed by HB, it is only the total amount of deformation applied up to a given time that enters into the determination of the hydrodynamic state of the frontal zone. A useful measure of this quantity is the deformation length scale L_d defined as

$$L_d(t)=L_0e^{-\int_0^t\alpha(t')dt'} \tag{8}$$

or in our special case:

$$L_d(t)=L_0e^{-\alpha_0 t}. \tag{9}$$

The constant L_0 is the initial width of frontal zone and is arbitrary, as long as it is large compared to the Rossby radius of deformation. For this paper, L_0 = 8000 km was chosen.

For the choice of a height-independent deformation field, one can show (HB) that the evolution of the frontal zone is described by functions of the form:

$$\bar{U}=U_d(x,t)+U_{\mathrm{HB}}(x,z,t) \tag{10}$$

$$\bar{V}=V_d(y,t)+V_{\mathrm{HB}}(x,z,t) \tag{11}$$

$$\bar{W}=W_{\mathrm{HB}}(x,z,t) \tag{12}$$

$$\bar{\Theta}=\Theta_{\mathrm{HB}}(x,z,t) \tag{13}$$

$$\bar{\phi}=\phi(x,z,t)+f\alpha xy-\alpha^2\frac{y^2}{2}-V_{\mathrm{HB}}{}^2(x,z,t)/2. \tag{14}$$

Hoskins and Bretherton transformed the nonlinear problem described by (2)–(5) and (10)–(14) into a linear one through the introduction of the "geostrophic" coordinates:

$$X=x+V_{\mathrm{HB}}/f$$

$$Z=z. \tag{15}$$

Initially the horizontal temperature gradient is so weak that $V_{\mathrm{HB}} \approx 0$ and as a result:

$$X(t=0)=x$$

$$Z(t=0)=z. \tag{16}$$

From Kelvin's circulation theorem, HB were able to show that X obeys the following evolution equation:

$$\frac{DX}{Dt}=-\alpha X. \tag{17}$$

In the (X, Z) space, the thermal wind relation requires that

$$f\frac{\partial}{\partial Z}V_{\mathrm{HB}}=\frac{g}{\Theta_0}\frac{\partial}{\partial X}\Theta_{\mathrm{HB}}. \tag{18}$$

Similarly the vertical component of absolute vorticity is

$$\zeta=\frac{f}{1-(1/f)(\partial V_{\mathrm{HB}}/\partial X)}. \tag{19}$$

From (14) and (18), one can show that

$$fV_{\mathrm{HB}}=\frac{\partial\phi}{\partial X} \quad \text{and} \quad \frac{g}{\Theta_0}\Theta_{\mathrm{HB}}=\frac{\partial\phi}{\partial Z}. \tag{20}$$

Ertel's potential vorticity q in the (X, Z) space is

$$q=\frac{1}{r}\zeta\frac{\partial\Theta_{\mathrm{HB}}}{\partial Z}. \tag{21}$$

Because the fluid is inviscid and adiabatic, q is conserved following parcel trajectories. If we adopt a Lagrangian viewpoint and define

$$((X_0(X,Z,t), Z_0(X,Z,t))$$

as the initial position of the parcel now at (X, Z), then

$$q(X,Z,t)=q(X_0,Z_0,0). \tag{22}$$

Furthermore, Θ_{HB} is also conserved following fluid motion and hence

$$\Theta_{\mathrm{HB}}(X,Z,t)=\Theta_{\mathrm{HB}}(X_0,Z_0,0). \tag{23}$$

From (17), a third Lagrangian constraint

$$X=X_0e^{-\alpha_0 t} \tag{24}$$

is obtained. The substitution of (19) and (20) into (21) results in the following elliptic equation for ϕ:

$$\frac{1}{f^2}\frac{\partial^2\phi}{\partial X^2}+\frac{1}{N^2}\mu\frac{\partial^2\phi}{\partial Z^2}=1, \tag{25}$$

where N^2 is the Brunt–Väisälä frequency defined by

$$N^2 = \frac{g}{f\theta_0} r(Z_0) q \tag{26}$$

and μ is the ratio of initial to present pseudodensity:

$$\mu = \frac{r(Z_0)}{r(Z)}. \tag{27}$$

From (22) and (26), we note that

$$N^2(X, Z, t) = N^2(X_0, Z_0, 0). \tag{28}$$

The horizontal boundaries of the fluid are fixed at the ground $Z = 0$ and along a constant pressure surface, high up in the stratosphere. Following H, we will take this upper boundary to be the 135 mb surface which is at a height of approximately Z_s = 12 km. Along these boundaries, the vertical velocity vanishes and parcels initially on them are constrained to remain there. Hence the conservation of potential temperature (23) implies that

$$\left.\begin{aligned} \Theta_{HB}(X, 0, t) &= \Theta_{HB}(X_0, 0, 0) \\ \Theta_{HB}(X, Z_s, t) &= \Theta_{HB}(X_0, Z_s, 0) \end{aligned}\right\}. \tag{29}$$

The domain is unbounded in X, and far from the front the horizontal temperature gradient is assumed to vanish, that is,

$$\frac{\partial \Theta_{HB}}{\partial X} \to 0 \quad \text{as} \quad |X| \to \infty. \tag{30}$$

One can use (20) to express these boundary conditions in terms of ϕ:

$$\frac{\partial \phi}{\partial Z}(X, Z, t) = \frac{g}{\Theta_0} \Theta_{HB}(X_0, Z, 0) \quad \text{at} \quad Z = 0 \text{ and } 12\,\text{km} \tag{31}$$

and

$$\frac{\partial \phi}{\partial X} \to 0 \quad \text{as} \quad |X| \to \infty. \tag{32}$$

To close the problem, the initial distributions of potential vorticity $q(X_0, Z_0, 0)$ and potential temperature $\Theta_{HB}(X_0, Z_0, 0)$ must be specified. They are related by (21) which at $t = 0$ reduces to:

$$\frac{\partial \Theta_{HB}}{\partial Z_0} = \frac{r(Z_0)}{f} q. \tag{33}$$

Integration of (33) gives the initial distribution of potential temperature:

$$\Theta_{HB}(X_0, Z_0, 0) = \Theta_i(X_0) + \frac{1}{f} \int_0^{Z_0} r(Z_0') q(X_0, Z_0', 0) dZ_0'. \tag{34}$$

The initial surface temperature distribution is given by $\Theta_i(X_0)$. An additional constraint is provided by the requirement that the upper boundary of the domain has a constant temperature, i.e.,

$$\Theta_{HB}(X, Z_s, t) = \Theta_s. \tag{35}$$

This constraint ensures that there is no frontogenesis along this boundary. The choices for initial potential vorticity and surface temperature distributions will be discussed in the following section.

The determination of the hydrodynamic state of the frontal zone at any time t, or equivalently at any deformation scale L_d, has been reduced to the solution of (25) subject to boundary conditions (31) and (32). The coefficients in (25) require knowledge of the potential vorticity distribution q, or equivalently N^2. To determine these, one must know the initial position (X_0, Z_0) of the parcel now at (X, Z). The horizontal displacement X_0 of a parcel is the result of the action of the deformation field and it is given by (24). Knowledge of the vertical displacement Z_0 is not available beforehand and it must be solved for simultaneously with ϕ.

The following iterative producedure was employed to determine Z_0 and ϕ. Given an estimate of the vertical parcel displacement:

$$Z_0 = Z_0^{\nu}(X, Z, t), \tag{36}$$

the elliptic equation (25) is solved for $\phi^{\nu+1}$. From (20), $\Theta_{HB}^{\nu+1}$ can then be found. If we define our new and as yet undetermined estimate of the vertical parcel displacement as $Z_0^{\nu+1}$, then the conservation of potential temperature (24) requires that

$$\Theta_{HB}(X_0, Z_0^{\nu+1}, 0) = \Theta_{HB}^{\nu+1}(X, Z, t), \tag{37}$$

This relation can be solved for $Z_0^{\nu+1}$. A consistent solution has been found if, and only if,

$$Z_0^{\nu+1}(X, Z, t) = Z_0^{\nu}(X, Z, t). \tag{38}$$

The procedure described above is repeated until (38) is satisfied to the required degree of accuracy. This Lagrangian approach is highly efficient and removes the necessity to integrate the conservation equations. With an initial guess $Z_0^0 = Z$, convergent solutions were always found in less than ten iterations.

Once a consistent solution $\phi(X, Z, t)$ and $Z_0(X, Z, t)$ has been determined, (20) can be used to find $V_{HB}(X, Z, t)$ and $\Theta_{HB}(X, Z, t)$. The inverse of (15) is then applied to transform these fields back to the physical space.

One of the advantages of the semigeostrophic approximation is that the determination of the cross-frontal circulation U_{HB} and W_{HB} is separated from that for V_{HB} and Θ_{HB}. The continuity equation (6) can be used to define a pseudo-streamfunction Ψ by

$$U_{HB} = \frac{1}{r} \frac{\partial \Psi}{\partial Z} \quad \text{and} \quad W_{HB} = -\frac{1}{r} \frac{\partial \Psi}{\partial X}. \tag{39}$$

Substitution of (39) into (2)–(5) and transformation to semigeostrophic space yields the following elliptic equation for Ψ.

$$\frac{\partial}{\partial X}\left(\frac{q}{f}\frac{\partial}{\partial X}\Psi\right)+\frac{\partial}{\partial Z}\left(\frac{f^2\Theta_0}{gr}\frac{\partial}{\partial Z}\Psi\right)=-2\alpha\frac{\partial\Theta_{HB}}{\partial X}. \quad (40)$$

The boundary conditions on Ψ are

$$\Psi=0 \quad \text{at} \quad Z=0 \quad \text{and} \quad Z=Z_s \quad (41)$$

$$\Psi\to 0 \quad \text{as} \quad |X|\to 0. \quad (42)$$

Once Z_0 and Θ_{HB} have been determined, (40) can be solved to find Ψ; U_{HB} and W_{HB} can then be found from (39).

In the Boussinesq approximation, one assumes that the vertical particle displacements are small compared with the scale height of the atmosphere. This is equivalent to assuming that μ, as defined in (26), is unity. In the constant potential vorticity model, the Boussinesq approximation is crucial for it eliminates the need for knowledge of Z_0 and allows for the analytic solution described by HB to be found. In the continuous model, we require knowledge of Z_0 to determine the potential vorticity distribution and hence this approximation is not essential. The retention of μ in (25) is equivalent to assuming that the fluid is anelastic. This case was referred to by H as being non-Boussinesq. We will consider the frontal zones that form in both Boussinesq and anelastic fluids.

3. The initial states

From section 2, we note that the specification of the initial state requires the definition of both the initial potential vorticity and temperature fields. In the atmosphere, the troposphere and stratosphere have widely different Brunt–Väisälä frequencies and are separated by a transition layer that is known as the tropopause. Fronts form in regions in which there is a temperature contrast along the surface. Our choices for the initial potential vorticity distribution and potential temperature distribution along the boundaries were chosen so as to satisfy these requirements. In addition, the possibility of either a barotropic or a localized perturbation to the initial state was allowed for. A distribution of the form:

$$q(X_0,Z_0,0)=\frac{\nu^2+1}{2r(Z_0)}+\frac{(\nu^2-1)}{2r(Z_0)}\tanh[(Z_0-Z_t)/\delta]+q_l'(X_0,Z_0) \quad (43)$$

was used for the initial potential vorticity field. The parameter ν^2 represents the ratio of stratospheric to tropospheric stratification and it was fixed at 9. The depth of the transition zone δ is a free parameter and it will be varied so as to determine its effect on the fronts that form. The possibility of a localized perturbation to the initial state is allowed for by the inclusion of $q_l'(X_0, Z_0)$. From (34) the potential temperature distribution consistent with (43) is

$$\Theta_{HB}(X_0,Z_0,0)=\Theta_i(X_0)+\frac{(\nu^2+1)}{2}Z_0+\frac{(\nu^2-1)}{2}\delta\log\left[\frac{\cosh(Z_0-Z_t)/\delta}{\cosh Z_t/\delta}\right]+\frac{1}{f}\int_0^{Z_0}r(\tilde{Z}_0)q_l'(X_0,\tilde{Z}_0)d\tilde{Z}_0. \quad (44)$$

The surface temperature distribution of the form

$$\Theta_i(X_0)=\frac{R}{\pi}\tan^{-1}X_0+\Theta_b'(X_0) \quad (45)$$

was employed. The parameter R denotes the cross-front surface temperature contrast. The possibility of a barotropic temperature perturbation is allowed for by the inclusion of $\Theta_b'(X_0)$. We note that if $\Theta_b' = 0$, then the Θ_i is a monotonic increasing function of X_0. The mean tropopause height Z_t is determined by the requirement that (35) is satisfied, i.e.

$$\Theta_s=\Theta_{HB}(X_0,Z_s,0).$$

Substitution of (44) into the above yields Z_t as a function of X_0.

As discussed in section 1, the inclusion of a localized perturbation to the initial state is meant to model the additional frontogenetic action that results from cold-air advection. This effect will be allowed for by defining q_l' such that the initial state has a localized region in which the potential temperature is a minimum. Outside of this region, the initial state will be undisturbed. The following functional form for $q_l'(X_0, Z_0)$ satisfies the above requirements:

$$q_l'(X_0,Z_0)=0 \quad \text{for} \quad |Z_0-Z_c|>\delta Z_c$$

$$=\frac{\theta_l\pi}{4\delta Z_c}f(X_0)\cos\frac{\pi(Z_0-Z_c)}{2\delta Z_c} \quad \text{for} \quad |Z_0-Z_c|\leqslant\delta Z_c. \quad (46)$$

Its horizontal dependence is given by $f(X_0)$ which is defined by

$$f(X_0)=0 \quad \text{for} \quad |X_0-X_c|>\delta X_c$$

$$f(X_0)=\frac{1}{2}\left[1+\cos\frac{\pi(X_0-X_c)}{\delta X_c}\right] \quad \text{for} \quad |X_0-X_c|\leqslant\delta X_c. \quad (47)$$

Thus, we see that the localized perturbation is centered at (X_c, Z_c) and has a width and height of $2\delta X_c$ and $2\delta Z_c$, respectively. The magnitude of the resultant temperature perturbation is θ_l.

As was the case in Hoskins et al. (1984), the barotropic perturbation to the initial state represents the fact that the environment in which the front forms

may include the remnants of previous fronts. This will be modeled by including perturbations of the form

$$\Theta_b'(X_0) = \Theta_b f(X_0). \tag{48}$$

The magnitude of the perturbation is Θ_b and its horizontal extent $f(X_0)$ is given by (47). Thus we see that the barotropic perturbation is centered at X_c, has a width of $2\delta X_c$ and extends throughout the depth of the fluid.

The vertical profiles of the initial potential vorticity and temperature distributions are illustrated in Fig. 1. The troposphere and stratosphere have constant, but very different, potential vorticities. The change in stratification across the tropopause is apparent in the potential temperature profile. The depth of the transition layer (tropopause) is determined by δ, and profiles are shown for δ = 1.6 km and 4 km. Also shown in this figure is the profile for the case with δ = 1.6 km that results from the inclusion of a localized cold perturbation of $\Theta_l = -4.8°$ that is centered at Z_c = 6 km and with a depth of δZ_c = 1.6 km. With this choice of parameters, the perturbation is localized to the upper troposphere where it is associated a minimum in the potential vorticity.

The surface potential temperature and mean tropopause height distributions in the semigeostrophic space are shown in Fig. 2 for a deformation length scale L_d = 170 km. Recall that these two distributions are related through (35). The unperturbed potential vorticity profile with δ = 1.6 km, and illustrated in Fig. 1, was used to generate the mean tropopause height distribution. The effect that the inclusion of a barotropic cold perturbation of $\Theta_b = -4.8$°C centered at $X_c = -200$ km and with a width δX_c = 500 km is also illustrated. As discussed in section 1, the cold perturbation results in a relative minimum in the surface temperature distribution and a corresponding fold in the tropopause. It was this type of perturbation that resulted in the very intense upper-level front in H (compare Fig. 7 of H with Fig. 2). It should be noted that a cross-front temperature contrast of 24°C was used to generate the distributions in Fig. 2, while contrasts of 39° or 48°C were employed by H. As mentioned before, the contrasts used by H were much too large.

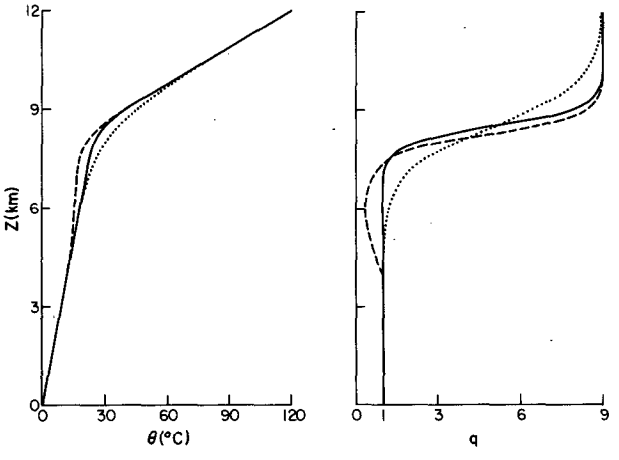

FIG. 1. The vertical profiles of potential temperature (Θ) and the potential vorticity (q) used in this paper. The solid and dotted lines denote the profiles with transition zone depths δ = 1.6 and 4 km, respectively. The dashed line indicates the changes in the δ = 1.6 km profile that result from the inclusion of a localized cold perturbation centered at Z_c = 6 km and with a depth δZ_c = 1.6 km. The magnitude of the temperature perturbation is $\Theta_l = -4.8$°C.

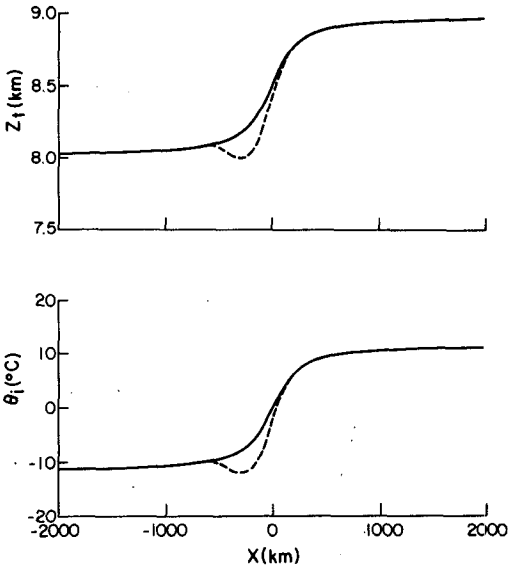

FIG. 2. The cross-front surface temperature (θ_t) and related tropopause height (Z_t) distributions used in this paper. The total cross-front temperature contrast R = 24°C. The solid lines denote the monotone increasing distribution. The dashed lines denote the distribution that results from the inclusion of a barotropic cold perturbation centered at $X_c = -200$ km and with a width δX_c = 500 km. The magnitude of the perturbation is $\Theta_b = -4.8$°C.

4. Results

In this section we will describe the frontal zones that form in the continuous model. First of all a comparison will be made with the two-layer model of H. After establishing the similarity of the two models, we will proceed to consider the fronts that form when there is a smaller and more realistic cross-front temperature contrast in the initial state. We will also discuss the effects that the inclusion of either a barotropic or localized perturbation has on the model. As was the case in H, we will identify the stages in the frontal evolution by use of the deformation length scale L_d as defined in (9). Once the initial state and L_d have been specified, the hydrodynamic state of the front was determined by the Lagrangian method outlined in section 2. The domain is unbounded in the cross-front direction. It was approximated by a finite domain with boundaries sufficiently distant from the front that their effect on

it was minimal. For the purposes of this paper, a domain of width 4000 km was employed. The elliptic equation (24), now defined on a finite domain, were solved with a direct method as implemented in the NCAR subroutine LIPTIC. A 40 × 40 grid was used, this corresponds to a horizontal resolution of 100 km and a vertical resolution of 0.3 km. We will concentrate primarily on the structure of the upper-level fronts. The surface fronts form in regions of constant potential vorticity and hence, are adequately described by the two-layer, or even the one-layer, model.

In Table 1, a comparison of several indicators of frontal intensity in the two-layer and continuous models is made. The comparison is made for a cross-front temperature contrast of 39° at L_d = 262 km and L_d = 170 km. The data for the two-layer model is from H. The depth of the transition layer δ in the continuous model was varied so as to determine its effect on frontal intensity. There is an actual discontinuity in the two-layer model, and hence, one would expect that the fronts that form in it to be more intense than those in the continuous model. In fact, the two-layer model can be thought of as the limiting case as $\delta \to 0$ in the continuous model. These statements are corroborated by the data in Table 1. As the transition zone becomes shallower, the upper-level front becomes more intense. Because of finite vertical resolution, values of δ less than 0.8 km were not considered. In Fig. 3, the potential temperature field Θ_{HB} and the along-front velocity field V_{HB} in the continuous model at L_d = 170 are displayed. The depth of the transition zone is δ = 1.6 km. Comparison of this figure with Fig. 9 in H shows that both models develop frontal zones with the same general characteristics. In particular, the frontal zones have a very strong surface front and a less intense upper-level front that is associated with an intrusion of stratospheric air into the troposphere. In both models, the surface front has become sufficiently intense so as to result in a breakdown in the coordinate transformation (15).

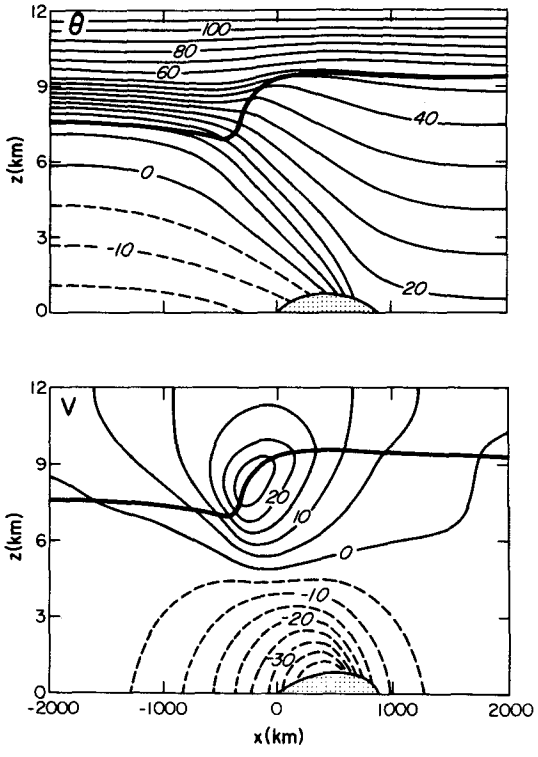

FIG. 3. The potential temperature field θ (°C) and the along-front velocity field V (m s^{-1}) associated with the frontal zone in the continuously stratified boussinesq fluid for the case R = 39°C and δZ_c = 1.6 km at L_d = 170 km. The position of the mean tropopause is denoted by the heavy line. The coordinate transformation from semigeostrophic to physical space has broken down in the stippled region.

TABLE 1. A comparison of the intensity of the upper-level front in the two-layer and continuous models for a cross-front temperature contrast of 40°. The data for the two-level model is taken from H.

	Two-layer model	Continuous model		
		L_d = 262 km		
		δ = 0.8 km	δ = 1.6 km	δ = 4 km
V_{max} (m s^{-1})	36	26	26	21
ζ_{max}	1.8f*	1.5f	1.4f	1.3f
Tropopause descent (mb)	40	34	32	27
		L_d = 170 km		
		δ = 0.8 km	δ = 1.6 km	δ = 4 km
V_{max} (m s^{-1})	41	31	29	25
ξ_{max}	2.5f*	1.8f	1.6f	1.4f
Tropopause descent (mb)	65	61	59	43

* In the two-layer model, the vorticity is discontinuous across the tropopause. An average value has been used.

Having demonstrated the similarity of the two-layer and continuous models for the case of a cross-front temperature contrast of 39°C, we will now proceed to consider the fronts that form with smaller and more realistic contrasts. Figure 4 shows the Θ_{HB} and the V_{HB} fields at L_d = 170 km for the fluid with δ = 1.6 km and a 24°C contrast. Comparison of Figs. 3 and 4 show that both surface and upper-level fronts in the present case are much less intense. The reduction in intensity of the surface front has eliminated the region in which (15) is invalid, while for the upper-level front it has resulted in the absence of a deep tropopause fold. In fact, the maximum tropopause depression is only 24 mb (as compared to 61 mb in the 39°C case).

In H, a cold barotropic perturbation was shown to greatly enhance upper-level frontogenesis. A similar perturbation was described in section 2, and the frontal zone that evolved on the initial state that included it is illustrated in Fig. 5. Comparison of Figs. 4 and 5 show that the intensity of the upper-level front has been

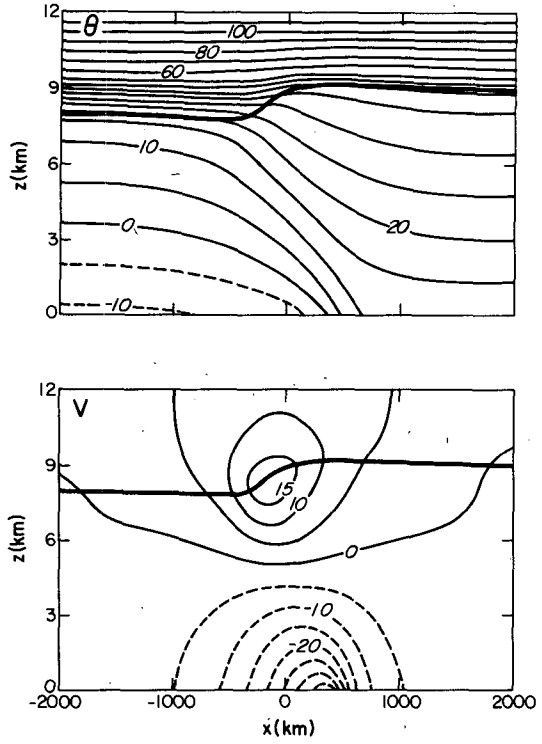

FIG. 4. As in Fig. 3 but for the case R = 24°C.

greatly increased and a deep tropopause fold has developed. Indicators of the strength of the upper-level front that develop on the unperturbed and perturbed initial states are listed in Table 2. Although not explicitly mentioned by H, the inclusion of a barotropic perturbation also resulted in an increase in the intensity of the surface front. In the particular case under investigation, it has led to a breakdown in the coordinate transformation (15) in the vicinity of the surface front. This has been indicated in Fig. 5.

Several factors contribute to the relative weakness of the upper-level front as compared to the surface front. These include the assumption that the fluid is Boussinesq; that the deformation field is independent of height; and that the front is two-dimensional. Hoskins (1972) considered the fronts that form in a two-layer anelastic model and found that this led to a slight redress in the imbalance. The fronts that form in a continuous anelastic model will be discussed below. The large-scale baroclinic waves that provide the deformation have their maximum amplitude at upper levels, and hence the actual deformation field most probably has a similar maximum. In addition, the inclusion of dissipative effects would act to reduce the strength of the deformation field near the surface. Such a height dependent deformation field would result in more intense upper-level fronts. Unfortunately, it leads to a three-dimensional problem that is not amenable to the present analysis scheme. The growing baroclinic wave also produces shearing deformation in addition to the stretching deformation considered in this paper. Based on work by Shapiro (1981), Keyser and Pecnick (1985) demonstrated that the inclusion of a shearing deformation field, in a primitive equation model, could result in an intensification of the upper-level front. Their choice of a shearing field was a particularly simple one that resulted in a two-dimensional problem. A more general field again results in a three-dimensional problem. From similar arguments Buzzi et al. (1981) concluded that upper-level frontogenesis is an intrinsically three-dimensional process that cannot be effectively studied in a two-dimensional context. As described above, there is an intermediate stage that can be exploited with the continuous model. We can include a localized perturbation that models the cold air advection mechanism identified by Keyser and Pecnick (1985). It should be reiterated that this type of perturbation requires a local modification to the potential vorticity field and as a result it cannot be included in a two-layer model.

The frontal zone that evolved on the initial state with the localized perturbation described in section 2 is illustrated in Fig. 6. The deformation length scale used was L_d = 170 km and the depth of the transition layer was set at 1.6 km. As described above, this particular perturbation resulted in a potential temperature minimum in the upper troposphere and is meant to

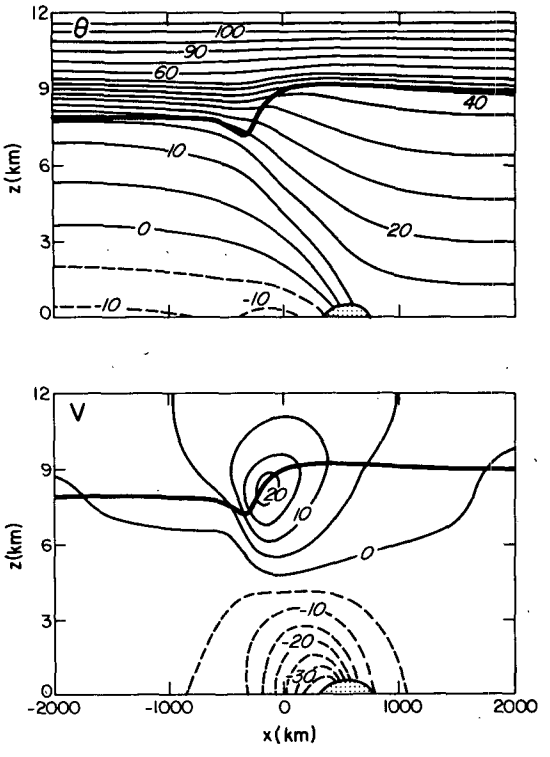

FIG. 5. As in Fig. 4 but for the initial state that includes the cold barotropic perturbation described in the text.

TABLE 2. A comparison of the intensity of the upper-level front that develops on the unperturbed initial state with those that develop on perturbed initial states (L_d = 170 km, δ = 1.6 km, R = 24°)

	Unperturbed initial state (Boussinesq)	Initial state with barotropic perturbation (Boussinesq)	Initial state with localized perturbation (Boussinesq)	Initial state with localized perturbation (anelastic)
V_{max} (m s^{-1})	19	22	22	28
ξ_{max}	$1.34f$	$1.75f$	$1.65f$	$2.01f$
Tropopause descent (mb)	24	62	64	85

model the local advection of cold air by the upper-level jet. Comparison of Figs. 4 and 6 indicate that its inclusion has greatly intensified the upper-level front and a deep tropopause fold has developed. Because the perturbation is localized to the upper troposphere, it has no effect on the surface front. Thus, unlike the barotropic perturbation, it has led to a substantial redress in the imbalance of intensity between the surface and upper-level front.

Table 2 compares the intensity of the upper-level fronts that develop on the unperturbed initial state with those that develop on the initial state with either the barotropic or localized perturbation. From this table, we see that the upper-level fronts that form on the perturbed initial states have roughly the same intensity and comparison of Figs. 5 and 6 show that they have the same basic characteristics.

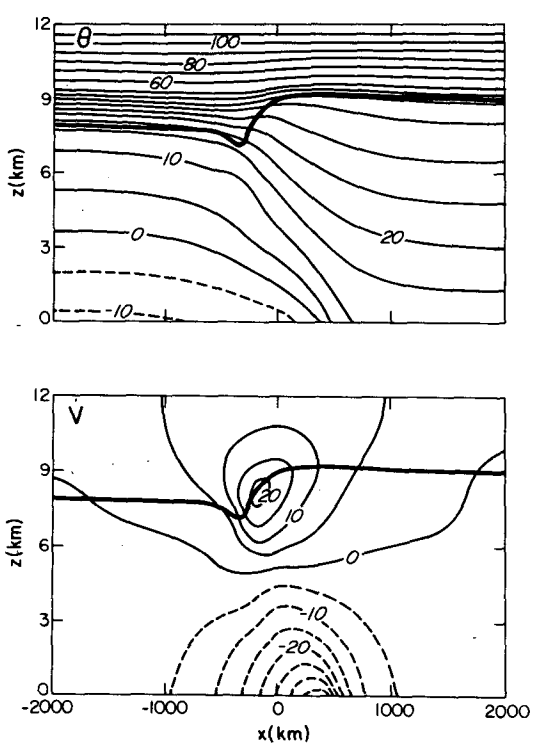

FIG. 6. As in Fig. 4 but for the initial state that includes the cold localized perturbation described in the text.

Consideration of the cross-front circulation equation (40) gives an explanation as to why the inclusion of a cold perturbation, either barotropic or localized, results in an intensification of the upper-level front. The sign of the inhomogeneous term in (40) gives the sense of the cross-front circulation. In the unperturbed case, $\partial\Theta_{HB}/\partial x$ is positive throughout the domain and this results in the broad counterclockwise circulation described by H. The inclusion of a cold perturbation results in a region in which $\partial\Theta_{HB}/\partial x$ is negative. Across this region, (40) requires that the circulation be clockwise. In the case of a barotropic perturbation, this additional frontogenetic process is felt throughout the depth of the fluid and results in the intensification of both the surface and upper-level front. By contrast, in the case of the localized perturbation it only has an effect on the upper-level front.

Hoskins (1972) considered the frontal zones that developed in an anelastic two-layer model. He concluded that the surface fronts were weaker and the upper-level fronts were stronger than the corresponding fronts in a Boussinesq model. An analogous result was found in the continuous model. Figure 7 displays a frontal zone that developed in a continuously stratified anelastic fluid. All parameters are the same as for the case illustrated in Fig. 6. Table 2 also includes the indicators for the upper-level front in the anelastic model.

5. Conclusions

In this paper, we have used the geostrophic momentum approximation to consider the nature of the frontal zones that result from the action of a stretching deformation field in a continuously varying potential vorticity fluid. In such a fluid, potential vorticity is conserved following parcel trajectories. As these trajectories are not known beforehand, this class of problem is difficult to solve using an Eulerian approach (Buzzi et al. 1981). By adopting a Lagrangian viewpoint, we have been able to develop a simple iterative procedure that results in both the parcel trajectories and the hydrodynamic state of the frontal zone at any given time in its evolution.

In such a model, the tropopause is represented as a shallow region over which the potential vorticity changes from a representative tropospheric value to a representative stratospheric one. The depth of this

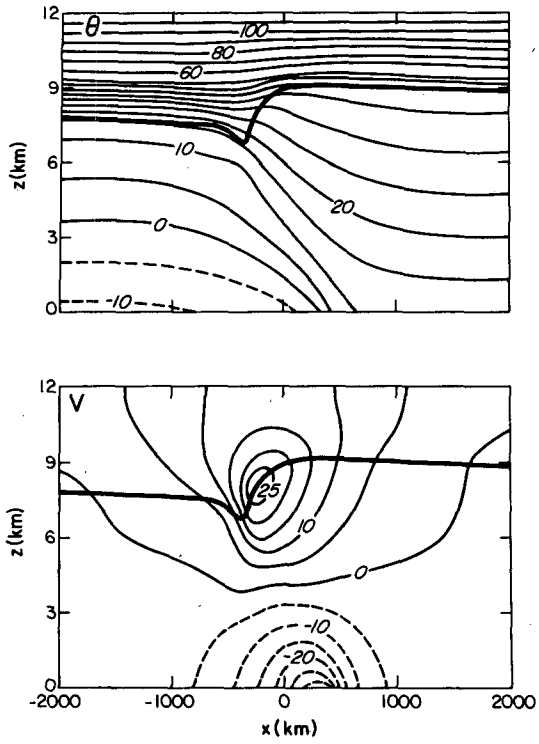

FIG. 7. As in Fig. 6 but for the anelastic fluid.

transition zone can be varied, so as to determine its effect on the fronts that form.

Hoskins et al. (1984) have shown that localized perturbations in the initial state may have substantial effects on the process of frontogenesis. In a constant or two-layer potential vorticity fluid, the only type of perturbation that can be considered is one that is localized in the cross-front direction but that extends throughout the depth of the fluid. In a continuously varying potential vorticity fluid, one is also able to consider perturbations that are localized in both spatial directions. These two types of perturbations were referred to as barotropic and localized, respectively.

For the initial states used by H, we found good agreement between our model and the two-layer model. We found that a reduction in the depth of the transition zone resulted in an increase in the intensity of the upper-level front. The two-layer model can be considered as the limiting case in which the transition zone depth tends to zero in the continuous model.

The initial states employed by H had surface cross-front temperature contrasts that were unrealistically large. The fronts that formed on initial states with smaller, and more realistic, contrasts were much less intense. In particular we found no evidence of a deep tropopause fold.

A cold barotropic perturbation was shown by H to dramatically increase the intensity of the upper-level front in the two-layer model and to result in the development of a deep tropopause fold. We also found this to be the case in the continuous model. However, this type of perturbation also led to an increase in the intensity of the surface front. For the case considered, it resulted in a breakdown in the co-ordinate transformation between the semigeostrophic and the physical space in the vicinity of the surface front.

Keyser and Pecnick (1985) have identified the upper-level advection of cold air by the upper-level jet as an additional frontogenetic process. This advection results in a region of reduced potential temperature that is localized to the region of the jet. We have shown that a localized perturbation with this property results in an increase in the intensity of the upper-level front. The behavior of this type of perturbation was very different from that associated with the barotropic perturbation.

REFERENCES

Buzzi, A., A. Trevison and G. Salustri, 1981: Internal frontogenesis: A two-dimensional model in isentropic, semigeostrophic coordinates. *J. Atmos. Sci.*, **109,** 1053–1060.

Hoskins, B. J., 1971: Atmospheric frontogenesis models: Some solutions. *Quart. J. Roy. Meteor. Soc.*, **97,** 139–153.

——, 1972: Non-Boussinesq effects and further development in a model of upper tropospheric frontogenesis. *Quart. J. Roy. Meteor. Soc.*, **98,** 532–541.

——, 1975: The geostrophic momentum approximation and the semigeostrophic equations. *J. Atmos. Sci.*, **32,** 233–242.

——, and F. P. Bretherton, 1972: Atmospheric frontogenesis models: Mathematical formulation and solution. *J. Atmos. Sci.*, **29,** 11–37.

——, E. C. Neto and H. R. Cho, 1984: The formation of multiple fronts. *Quart. J. Roy. Meteor. Soc.*, **110,** 881–896.

Keyser, D., and M. J. Pecnick, 1985: A two-dimensional primitive equation model of frontogenesis forced by confluence and horizontal shear. *J. Atmos. Sci.*, **42,** 1259–1282.

Palmen, E., and C. W. Newton, *Atmospheric Circulation Systems.* Academic Press, 1969.

Reed, R. J., 1955: A study of a characteristic type of upper-level frontogenesis. *J. Meteor.*, **12,** 226–237.

Shapiro, M. A., 1981: Frontogenesis and geostrophically forced secondary circulations in the vicinity of jet stream frontal zone systems. *J. Atmos. Sci.*, **38,** 954–973.

Stone, P. H., 1966: Frontogenesis by horizontal wind deformation fields. *J. Atmos. Sci.*, **23,** 455–465.

Williams, R. T., 1968: A note on quasi-geostrophic frontogenesis. *J. Atmos. Sci.*, **25,** 1157–1159.